Published in final edited form as:
Magn Reson Med. 2010 November ; 64(5): 1274–1280. doi:10.1002/mrm.22553.

The Biodistribution of [^{153}Gd]Gd-Labeled Magnetic Resonance Contrast Agents in a Transgenic Mouse Model of Renal Failure Differs Greatly from Control Mice

Thaddeus J. Wadas[1,*], **Christopher D. Sherman**[1], **Jeffrey H. Miner**[2], **James R. Duncan**[1], and **Carolyn J. Anderson**[1,3,4]

[1]Mallinckrodt Institute of Radiology, Washington University School of Medicine, St. Louis, MO USA

[2]Renal Division, Department of Internal Medicine, Washington University School of Medicine, St. Louis, MO USA

[3]Department of Biochemistry & Molecular Biophysics, Washington University School of Medicine, St. Louis, MO USA

[4]Department of Chemistry Washington University School of Arts and Sciences, St. Louis, MO, USA

Abstract

Nephrogenic Systemic Fibrosis (NSF) occurs in renally impaired patients who have undergone contrast enhanced MR examination using intravenous gadolinium (Gd)-based contrast agents. The effect of impaired kidney function on the biodistribution of Gd-based contrast agents was investigated using radiolabeled $^{153/Nat}$Gd-DOTA, $^{153/Nat}$Gd-DTPA and $^{153/Nat}$Gd-DTPA-BMA in a transgenic mouse model of renal impairment. Renally impaired (RI) animals had more activity associated with their tissues than did control mice, and this increase varied according to the radiotracer injected. For example, after 7 days, RI animals that received $^{153/Nat}$Gd-DOTA had 3-fold ($p < 0.037$) more activity in their bone tissue while RI animals receiving $^{153/Nat}$Gd-DTPA and $^{153/Nat}$Gd-DTPA-BMA had 8-fold ($p < 0.0001$) and 24-fold ($p < 0.0001$) more activity in their bone tissue, respectively. These findings demonstrate that renal impairment dramatically alters the tissue distribution of Gd^{3+} ions *in vivo*, which are likely a critical factor in the development of NSF.

Keywords

Nephrogenic Systemic Fibrosis; gadolinium; magnetic resonance imaging; Alport syndrome

Introduction

Nephrogenic Systemic Fibrosis (NSF) was first described in the literature by Cowper and coworkers in 2000, and since their initial publication, approximately 325 cases have been reported to the FDA and the NSF registry at Yale University (1–3). This disease manifests itself initially with redness, itching and swelling of the distal extremities followed by the formation of firm erythematous and indurated plaques of the skin associated with

[*]Address correspondence to: Thaddeus J. Wadas, Ph.D., Mallinckrodt Institute of Radiology, Washington University School of Medicine, 4940 Parkview Place, Campus Box 8225, St. Louis, MO 63110, Phone: 314-362-8441, Fax: 314-362-9940, wadast@wustl.edu.

subcutaneous edema (4). As the disease progresses, patients experience flexion contracture in the afflicted extremities with a limited range of motion, pain, paresthesia and/or severe pruritis. In addition to cutaneous manifestations, autopsy results suggest that NSF is a systemic disorder involving vital organs such as the lung, liver and heart (5). While the exact etiology of NSF remains to be identified, correlated clinical data taken from patients with NSF suggests that several factors stimulate the onset of this disease, and two factors seem to be most prevalent (6). All patients who developed NSF had been diagnosed with some form of renal impairment and they all received single or multiple doses of Gd-based contrast agents (GCAs). For example, Deo and coworkers looked at the incidence of NSF among patients with end stage renal disease (ESRD) from 2005–2006 and determined that all of the cases had occurred within 2 months of gadolinium exposure (7). Additionally, Markmann et al. identified 13 patients (age range 33 to 66 yrs) who had been diagnosed to have some form of NSF (8). Despite the differences in symptoms, all 13 patients had two criteria in common: they all suffered from ESRD, and they all had been exposed to GCAs. These observations have prompted several studies designed to describe the role GCAs and Gd^{3+} ions play in stimulating NSF development (9–11).

An understanding of how renal insufficiency affects the biodistribution of GCAs and NSF formation has not been adequately formulated. This lack of understanding is due in part to the lack of suitable animal models. While several animal models of renal impairment exist, their creation involves technically demanding surgical procedures or the systemic administration of nephrotoxins, which potentially have serious adverse side effects that might influence the outcome of the results of the intended study (12,13). Over a decade ago, transgenic mice with an engineered mutation in the *Col4a3* gene, which models the impaired renal function observed in human Alport syndrome, were generated (14–16). This disease is characterized by delayed onset of glomerulonephritis that progresses through gradual loss of kidney function and end stage renal failure. The goal of this study was to examine the role renal insufficiency plays in the biodistribution of Gd after intravenous GCA administration by examining the biodistribution of $^{153/Nat}$Gd-DOTA, $^{153/Nat}$Gd-DTPA and $^{153/Nat}$Gd-DTPA-BMA in the Alport mouse.

Materials and Methods

All work involving the use of radioactive materials at Washington University was conducted under Radiation Safety Committee approved authorizations in accordance with the University's Nuclear Regulatory Commission license. Gadolinium-153 ($t_{1/2}$ = 242 d, γ; 29.5%, $E\gamma_{max}$ = 97.43 keV, γ, 21.1%, $E\gamma_{max}$ = 103.2 keV) was obtained from Perkin Elmer Life and Analytical Sciences (Billerica, MA USA). All other chemicals were purchased from Sigma-Aldrich Chemical Co. (St. Louis, MO USA), and solutions were prepared using ultrapure water (18 MΩ-cm resistivity). 2,2',2",2"'-(2,2'-(carboxymethylazanediyl)bis(ethane-2,1-diyl)bis(azanetriyl))tetraacetic acid (DTPA) was obtained from Sigma-Aldrich Chemical Co. (St. Louis, MO USA), 1,4,7,10-Tetraazacyclododecane-1,4,7,10-tetraacetic acid (DOTA) was obtained from Macrocyclics (Dallas, TX USA), and 5,8-bis(carboxymethyl)-2-(2-(methylamino)-2-oxoethyl)-10-oxo-2,5,8,11-tetraazadodecane-1-carboxylic acid (DTPA-BMA) was generously provided by Covidien (Mansfield, MA USA). Radiochemistry reaction progress and purity were monitored by analytical radio-TLC, which was conducted on a Bioscan AR 2000 radio-TLC scanner equipped with a 10% methane:argon gas supply and a PC interface running Winscan v.3 analysis software. Silica plates were employed using an eluent mixture of 3:7 10% NaOAc:MeOH, and the complex $^{153}Gd(OAc)_3$ as a standard control. Radioactive samples were counted using a Perkin Elmer Wizard 3 automatic gamma counter purchased from Perkin Elmer Life and Analytical Sciences (Billerica, MA USA).

Animal Handling

Wild Type (WT) C57BL/6J mice (6–9 mo. of age) were obtained from The Jackson Laboratory (Bar Harbor, Maine USA). Renally impaired (RI) *Col4a3*−/− mice and *Col4a3*+/− (control) littermates (5–8 mo. of age) on the C57BL/6J strain background were housed under pathogen-free conditions according to the guidelines of the Division of Comparative Medicine, and the Animal Studies Committee of Washington University School of Medicine approved all experiments. Animals that were injected with radioactivity were housed in a separate facility, which was approved by the Washington University Radiation Safety Committee in accordance with the University's Nuclear Regulatory Commission license.

Serum Blood Urea Nitrogen Analysis

Blood samples were collected from RI and control mice via submandibular venous puncture and placed in serum separator tubes (Becton Dickinson). The blood samples were placed at 4 °C for 5 min, and then centrifuged at 10,000 RPM for 5 min. The serum was separated from the cellular fraction and stored at 0°C. The concentrations of blood urea nitrogen (BUN) in the serum were measured with a Cobas Mira Plus analyzer (Roche, Somerville, NJ). Due to the spontaneous nature of disease progression in *Col4a3*−/− mice, these animals exhibited BUN levels, which ranged from 30–100 mg/dl. Based upon previous observations, animals that had BUN levels of 30 mg/dl or greater were considered renally impaired and used in these studies (14,16).

Preparation of $^{153/Nat}$Gd-DOTA

The preparation of $^{153/Nat}$Gd-DOTA was accomplished by combining a 100 µl solution of $^{153/Nat}Gd(OAc)_3$ (0.8 mM, 2.6 MBq (70 µCi)) with 100 µl of a 1 mM solution of DOTA in 0.4 M NaOAc (pH 5.5). The resulting solution was heated for 60 min at 95 °C. $^{153/Nat}$Gd-DOTA was prepared in a 98±2% yield based on TLC analysis (n = 4 syntheses). The final specific activity was determined to be 325 MBq/µmol (Figure 1).

Preparation of $^{153/Nat}$Gd-DTPA

The preparation of $^{153/Nat}$Gd-DTPA was accomplished by combining a 100 µl solution of $^{153/Nat}Gd(OAc)_3$ (0.8 mM, 2.6 MBq (70 µCi)) with 100 µl of a 1 mM solution of DTPA in 0.4 M NaOAc (pH 5.5). The resulting solution was heated for 60 min at 95 °C. $^{153/Nat}$Gd-DTPA was prepared in a 98±1% yield based on TLC analysis (n = 3 syntheses). The final specific activity was determined to be 325 MBq/µmol (Figure 1).

Preparation of $^{153/Nat}$Gd-DTPA-BMA

The preparation of $^{153/Nat}$Gd-DTPA-BMA was accomplished by combining 100 µl $^{153/Nat}Gd(OAc)_3$ (0.8 mM, 2.6 MBq (70 µCi)) with 100 µl of a 1 mM solution of DTPA-BMA in 0.4 M NaOAc (pH 5.5). The resulting solution was heated for 60 min at 95 °C. $^{153/Nat}$Gd-DTPA-BMA was prepared in a 96±1% yield based on TLC analysis (n = 4 syntheses). The final specific activity was determined to be 325 MBq/µmol (Figure 1).

Biodistribution Studies

Biodistribution studies were conducted as previously described using standard protocols (17,18). Briefly, mice (5–9 months) were injected with $^{153/Nat}$Gd-DOTA, $^{153/Nat}$Gd-DTPA, or $^{153/Nat}$Gd-DTPA-BMA (0.12 MBq (3.5 nCi), 0.15 µg in 150 µL/mouse) via tail vein injection. Animals were sacrificed at selected time points post-injection (p.i.), and organs of interest were removed, weighed, and counted on a Perkin Elmer Wizard 3 automatic gamma counter. The percent-injected dose per gram (%ID/gram) and percent-injected dose per organ (%ID/organ) were calculated by comparison to a weighed, counted standard. All cohorts had a sample size of at least three animals, and each data point represents the mean

±SD of radioactivity accumulation in tissues harvested from a discrete cohort of mice at a particular time point.

Statistical Methods

All of the data are presented as mean±SD or mean (95% Confidence Interval). Statistical classifications routinely used to analyze biodistribution data were performed as previously described (19–25). Briefly, a student's t-test (two-tailed, unpaired) was used when comparing two groups (control vs. RI), while an one way Anova test, which was used to compare all three GCA's was performed using GraphPad Prism (San Diego, CA). Comparisons of data where $p < 0.05$ were considered significant.

Results

Biodistribution studies were performed on WT mice after the injection of $^{153/Nat}$Gd-DOTA, $^{153/Nat}$Gd -DTPA or $^{153/Nat}$Gd -DTPA-BMA, and the results obtained from analysis of the blood and selected tissues are presented in Figure 2. At very early time points the biodistribution of all three complexes were similar, and by 48 h all of the complexes were effectively cleared from the blood stream. Clearance from other tissues, however, was much slower over time, and this clearance was observed to be radiotracer dependent. For example, appreciable amounts of kidney associated activity were observed in animals receiving $^{153/Nat}$Gd-DTPA-BMA after 7 days (0.25±0.022 %ID/g) while the levels of tissue-associated activity in mice receiving $^{153/Nat}$Gd-DOTA (0.053±0.014 %ID/g) or $^{153/Nat}$Gd-DTPA (0.12±0.0011 %ID/g) were significantly lower ($p < 0.0001$).

Biodistribution experiments were also performed to examine the effects of renal impairment on the clearance profiles of $^{153/Nat}$Gd-DOTA, $^{153/Nat}$Gd-DTPA and $^{153/Nat}$Gd-DTPA-BMA at 24 hours and 7 days post-injection, and the results are presented in Figures 3 and 4. RI impaired mice were observed to have more tissue-associated radioactivity than their control counterparts, and this trend was consistent regardless of the radiotracer injected. For example, 24 h after $^{153/Nat}$Gd-DOTA was injected into RI and control animals, the amount of tissue-associated ^{153}Gd was 20-fold greater in the liver ($p = 0.002$) and 16-fold ($p < 0.0001$) greater in the spleen, while being 7-fold ($p = 0.0007$) greater in the kidney and 16-fold ($p = 0.0079$) greater in the bone when compared to control mice. For $^{153/Nat}$Gd-DTPA, 4-fold greater activity was observed in the liver ($p = 0.0218$), spleen ($p = 0.0280$) and kidney ($p = 0.0077$), while 6-fold ($p = 0.037$) greater activity was observed in the bone of RI mice when compare to control littermates. Finally, $^{153/Nat}$Gd-DTPA-BMA demonstrated the most prolonged clearance profile of the three radiotracers in RI mice. RI impaired mice injected with $^{153/Nat}$Gd-DTPA-BMA were observed to have 10-fold ($p < 0.0001$) more activity in liver, 15-fold ($p = 0.011$) more activity in spleen, 6-fold ($p = 0.008$) more activity in kidney and 44-fold ($p = 0.0008$) more activity in bone when compared to control animals at 24 h.

Although the amount of tissue-associated activity had decreased in RI and control animals after 7 days, significantly more activity was observed in the tissues of RI mice (Figure 3b). For example, RI mice that received $^{153/Nat}$ Gd-DOTA were observed to have 3-fold ($p < 0.022$) more activity in liver, 3-fold ($p = 0.028$) more activity in spleen, 7-fold ($p = 0.0077$) more activity in kidney and 3-fold ($p < 0.037$) more activity in bone than did their control littermates. Additionally, RI animals receiving $^{153/Nat}$Gd-DTPA demonstrated 6-fold ($p < 0.0001$) more activity in liver, 6-fold ($p = 0.0001$) more in spleen, 7-fold more ($p < 0.0006$) in kidney and 8-fold more ($p < 0.0001$) in bone than did their control littermates. Finally, animals receiving $^{153/Nat}$Gd-DTPA-BMA demonstrated 7-fold ($p < 0.0001$) more activity in liver, 6-fold ($p = 0.0037$) more activity in spleen, 5-fold ($p < 0.0001$) more activity in kidney, and 24-fold ($p < 0.0001$) more activity in bone.

Discussion

The role renal insufficiency plays in the formation of NSF has not been thoroughly examined. The purpose of these studies was to evaluate the biodistribution of $^{153/Nat}$Gd-DOTA, $^{153/Nat}$Gd-DTPA and $^{153/Nat}$Gd-DTPA-BMA, the main components in the contrast agents Dotarem®, Magnevist® and Omniscan®, respectively, in the context of renal impairment using a transgenic mouse model that spontaneously develops progressive renal failure 5–8 months after birth and has symptoms that are similar to human Alport syndrome.

Initially, biodistribution studies were conducted in WT mice, and although experiments similar to these have already been published using younger mice and radiolabeled kit formulations (26), they were necessary to ensure that the use of older animals and homogeneous solutions of the radiolabeled, carrier added complexes would not significantly alter the biodistribution profiles of each complex after injection. Biodistribution studies using radioactive labels such as ^{153}Gd allow for high sensitivity measurements to be obtained and are routinely used to evaluate the retention, clearance and stability of radiotracers *in vivo*. Additionally, the use of ^{153}Gd allows for a more facile measurement of metabolites and organ uptake in a cost effective manner and this should have broad appeal to researchers who do not have unfettered access to other techniques such as ICP-MS. All complexes demonstrated clearance profiles, which were similar to those reported previously (26); animals receiving $^{153/Nat}$Gd-DOTA retained the least amount of $^{153/Nat}$Gd, while$^{153/Nat}$Gd-DTPA demonstrated intermediate retention and $^{153/Nat}$Gd-DTPA-BMA had the highest retention of $^{153/Nat}$Gd in clearance organs and bone. These differences have been attributed to structural differences between the ligands and subsequent coordination complexes (9), and these findings are in agreement with the *in vivo* and *in vitro* work published by Tweedle and coworkers who used biodistribution studies in rats and mice and acid dissociation experiments to evaluate the kinetic stability of these three contrast agents (26,27).

Biodistribution studies involving RI and control mice 24 h and 7 d after radiotracer injection reveal how renal impairment alters the accumulation and clearance profiles of each Gd-complex *in vivo*. Renally impaired animals demonstrate greater uptake and retention of $^{153/Nat}$Gd than do their control littermates at both time points, regardless of injected radiotracer. Previously, a three-phase model has been offered to describe the tissue distribution and whole body retention of GCAs after injection (28). In the first phase, intact GCAs are excreted primarily through the urine, while the second phase involves Gd species being taken up in the liver and spleen where clearance is much slower than in the kidney. The final and slowest phase occurs with Gd being deposited into bone, from which the clearance may take years. Impaired renal function appears to significantly reduce the efficiency of the first phase of this model, increases the burden on the second two phases and provides the Gd a greater residence time *in vivo* and a greater opportunity to interfere with biochemical and cellular pathways. However, the nature of the Gd species in these tissues is currently unknown, may be tissue dependent and may include the intact contrast agents or any metabolized byproducts. For example, blood clearance is relatively rapid indicating that transchelation to proteins such as albumin does not occur, whereas clearance of activity from the livers of animals that received $^{153/Nat}$Gd-DTPA or $^{153/Nat}$Gd-DTPA-BMA is slow over time, and suggests that transchelation of the Gd^{3+} to cellular proteins may be occurring. Gd^{3+} ions have been observed to form complexes with proteins such as transferrin (29), which is a highly abundant liver protein, and several reports exist in the literature, which describe liver-localized radiometal transchelation after radiopharmaceutical injection (30,31). Moreover, Hocine et al. observed the presence of Gd in the lysosomes of Kupffer cells using histology and ion microscopy, suggesting that at least some concentration of the injected GCAs are being degraded *in vivo* (32), and these studies are in

agreement with those reported by Franano and colleagues (31). Additionally, Gd-DTPA-BMA demonstrated the greatest uptake in bone matrix and not the bone marrow over time, and this agrees with findings by Darrah et al. who analyzed femur samples of patients using inductively coupled plasma mass spectrometry (ICP-MS) (33). Since Gd^{3+} ions have a similar ionic radius to Ca^{2+} (107.8 pm vs. 114 pm) and are known to form coordination complexes with ligands such as PO_4^{3-}, which is abundant in the bone matrix material hydroxyapatite, the data suggest that the predominant Gd species is not protein bound but incorporated into the bone matrix. Metabolism studies will be required to elucidate the tissue-dependant nature of the Gd species *in vivo* and provide an understanding of what metabolites are generated, and where and when they are generated. Experiments are currently underway to answer these important questions.

Based upon the available clinical data, renal impairment is necessary for the development of NSF, but preclinical models that are useful in studying the pathophysiology of this disease have been lagging. Sieber et al. developed a preclinical model using normal rats, which received 20 injections of GCAs over the course of 4 weeks to create systemic concentrations of Gd similar to those observed in renally impaired patients. However, this model mimics the levels of Gd exposure rather than the impaired renal function found in patients with ESRD or acute kidney injury. While numerous animal models of renal failure exist, many involve manipulation of the animal's renal function using surgical or chemo toxic procedures, which can often produce unwanted side effects systemically. The transgenic mouse model used in these studies represents a useful alternative that will continue to be valuable in studying and understanding the role that renal insufficiency plays in the initiation and progression of NSF. Depending on the background strain, this animal model reaches impaired kidney function between 66 and 200 days, and the onset and progression of renal impairment can be easily monitored through routine blood sampling of creatinine and blood urea nitrogen levels. Finally, the renal pathology of this model closely mimics the pathology observed in human patients with renal disease.

Despite the use of this novel preclinical model for NSF, several issues should be considered when interpreting the presented data. Firstly, the number of transgenic animals that can be generated for use in any one experiment is relatively small when compared to the number of RI animals that can be generated using chemical or surgical manipulation. Secondly, due to the nature of the radiosynthesis using $^{153/Nat}Gd$, the injected mass of chelator was in 20% excess. The radio labeled injectates were not prepared from the commercially available or clinically used kit formulations, some of which contain excess chelator. For example, Omniscan® contains 5% excess of the Gd-free ligand, Ca-DTPA-BMA. Frenzel et al. examined the effects this had on the serum stability of these commercially available agents and determined that without the excess ligand, Gd release was much greater than when the excess ligand was present, especially in the presence of high phosphate concentration (34). In this study, the 20% excess of chelator may have imparted greater stability of the $^{153/Nat}Gd$-DTPA-BMA compared to the use of the commercially available kit. While the magnitude of Gd release may be higher than what was observed by Frenzel and coworkers, the data demonstrate that the model has the potential to be useful in the study of NSF. Finally, calculations estimate the concentration of any injected impurities to be at least 20 fold smaller than the concentration of the injected $^{153/Nat}Gd$ complexes. While an impurity may have some effect on the biodistribution data, these effects are believed to be minor. The fact that all three complexes have nearly identical biodistributions at early time points, demonstrate rapid clearance from the blood, and exhibit low spleen retention provides evidence to support the minimal role trace impurities may play in the tissue accumulation of Gd (35).

Conclusion

Nephrogenic Systemic Fibrosis is a debilitating disease that occurs in patients with impaired kidney function and that have been exposed to GCAs. While several studies have examined the role of GCA stability in NSF development, the role of impaired kidney function in the onset of NSF has not been thoroughly studied. Biodistribution studies in renally impaired mice demonstrate that renal impairment prolongs the residence time of the contrast agents in the organism, and this prolonged residence time allows for tissue dependent metabolism of the GCAs with release of the Gd^{3+} ion. Current efforts are underway to elucidate the identity of these metabolized species and the mechanisms, which stimulate the onset of NSF.

Supplementary Material

Refer to Web version on PubMed Central for supplementary material.

Acknowledgments

The authors gratefully acknowledge pilot grants from the International Society for Magnetic Resonance in Medicine and the Washington University George M. O'Brien Center for Kidney Disease Research (DK079333). The authors also acknowledge helpful discussions with Dr. Jon McConathy and Dr. F. Nicholas Franano, Proteon Therapeutics.

References

1. Sieber MA, Pietsch H, Walter J, Haider W, Frenzel T, Weinmann HJ. A preclinical study to investigate the development of nephrogenic systemic fibrosis: a possible role for gadolinium-based contrast media. Invest Radiol. 2008; 43(1):65–75. [PubMed: 18097279]
2. Cowper SE, Robin HS, Steinberg SM, Su LD, Gupta S, LeBoit PE. Scleromyxoedema-like cutaneous diseases in renal-dialysis patients. Lancet. 2000; 356(9234):1000–1001. [PubMed: 11041404]
3. Cowper, SE. Nephrogenic fibrosing dermopathy [NFD/NSF Website]. 2001–2009. http://www.icnfdr.org
4. Grobner T, Prischl FC. Gadolinium and nephrogenic systemic fibrosis. Kidney Int. 2007; 72(3): 260–264. [PubMed: 17507905]
5. Bhave G, Lewis JB, Chang SS. Association of gadolinium based magnetic resonance imaging contrast agents and nephrogenic systemic fibrosis. J Urol. 2008; 180(3):830–835. [PubMed: 18635232]
6. Swaminathan S, Shah SV. New insights into nephrogenic systemic fibrosis. J Am Soc Nephrol. 2007; 18(10):2636–2643. [PubMed: 17855637]
7. Deo A, Fogel M, Cowper SE. Nephrogenic systemic fibrosis: a population study examining the relationship of disease development to gadolinium exposure. Clin J Am Soc Nephrol. 2007; 2(2): 264–267. [PubMed: 17699423]
8. Marckmann P, Skov L, Rossen K, Dupont A, Damholt MB, Heaf JG, Thomsen HS. Nephrogenic systemic fibrosis: suspected causative role of gadodiamide used for contrast-enhanced magnetic resonance imaging. J Am Soc Nephrol. 2006; 17(9):2359–2362. [PubMed: 16885403]
9. Port M, Idee J-M, Medina C, Robic C, Sabatou M, Corot C. Efficiency, thermodynamic and kinetic stability of marketed gadolinium chelates and their possible clinical consequences: a critical review. BioMetals. 2008; 21(4):469–490. [PubMed: 18344005]
10. Sieber MA, Lengsfeld P, Frenzel T, Golfier S, Schmitt-Willich H, Siegmund F, Walter J, Weinmann H-J, Pietsch H. Preclinical investigation to compare different gadolinium-based contrast agents regarding their propensity to release gadolinium in vivo and to trigger nephrogenic systemic fibrosis-like lesions. Eur Radiol. 2008; 18(10):2164–2173. [PubMed: 18545998]
11. Edward M, Quinn JA, Mukherjee S, Jensen MBV, Jardine AG, Mark PB, Burden AD. Gadodiamide contrast agent 'activates' fibroblasts: a possible cause of nephrogenic systemic fibrosis. J Pathol. 2008; 214(5):584–593. [PubMed: 18220317]

12. Hewitson TD, Ono T, Becker GJ. Small animal models of kidney disease: a review. Methods Mol Biol. 2009; 466:41–57. [PubMed: 19148602]
13. Dai, C.; Kiss, L.; Liu, Y. Animal models of Kidney Disease. Conn, P., editor. Totowa, NJ: Humanna Press, Inc.; 2008. p. 657
14. Andrews KL, Mudd JL, Li C, Miner JH. Quantitative trait loci influence renal disease progression in a mouse model of Alport syndrome. Am J Pathol. 2002; 160(2):721–730. [PubMed: 11839593]
15. Cosgrove D, Kalluri R, Miner JH, Segal Y, Borza DB. Choosing a mouse model to study the molecular pathobiology of Alport glomerulonephritis. Kidney Int. 2007; 71(7):615–618. [PubMed: 17290292]
16. Miner JH, Sanes JR. Molecular and functional defects in kidneys of mice lacking collagen Î±3(IV): implications for Alport syndrome. J Cell Biol. 1996; 135(5):1403–1413. [PubMed: 8947561]
17. Boswell CA, Sun X, Niu W, Weisman GR, Wong EH, Rheingold AL, Anderson CJ. Comparative in vivo stability of copper-64-labeled cross-bridged and conventional tetraazamacrocyclic complexes. J Med Chem. 2004; 47(6):1465–1474. [PubMed: 14998334]
18. Sun X, Wuest M, Weisman GR, Wong EH, Reed DP, Boswell CA, Motekaitis R, Martell AE, Welch MJ, Anderson CJ. Radiolabeling and in vivo behavior of copper-64-labeled cross-bridged cyclam ligands. J Med Chem. 2002; 45(2):469–477. [PubMed: 11784151]
19. Sprague JE, Kitaura H, Zou W, Ye Y, Achilefu S, Weilbaecher KN, Teitelbaum SL, Anderson CJ. Noninvasive imaging of osteoclasts in parathyroid hormone-induced osteolysis using a ^{64}Cu-labeled RGD peptide. J Nucl Med. 2007; 48(2):311–318. [PubMed: 17268030]
20. Sprague JE, Peng Y, Sun X, Weisman GR, Wong EH, Achilefu S, Anderson CJ. Preparation and biological evaluation of copper-64-labeled Tyr3-octreotate using a cross-bridged macrocyclic chelator. Clin Cancer Res. 2004; 10(24):8674–8682. [PubMed: 15623652]
21. Lewis JS, Lewis MR, Srinivasan A, Schmidt MA, Wang J, Anderson CJ. Comparison of four ^{64}Cu-labeled somatostatin analogs in vitro and in a tumor-bearing rat model: Evaluation of new derivatives for positron emission tomography imaging and targeted radiotherapy. J Med Chem. 1999; 42(8):1341–1347. [PubMed: 10212119]
22. Beilvert A, Cormode DP, Chaubet F, Briley-Saebo K, Mani V, Mulder WJM, Vucic E, Toussaint JF, Letourneur D, Fayad ZA. Tyrosine polyethylene glycol (PEG)-micelle magnetic resonance contrast agent for the detection of lipid rich areas in atherosclerotic plaque. Magn Reson Med. 2009; 62(5):1195–1201. [PubMed: 19780153]
23. Mulder WJM, Strijkers GJ, Briley-Saboe KC, Frias JC, JGS A, Vucic E, Amirbekian V, Tang C, Chin PTK, Nicolay K, Fayad ZA. Molecular imaging of macrophages in atherosclerotic plaques using bimodal PEG-micelles. Magn Reson Med. 2007; 58(6):1164–1170. [PubMed: 18046703]
24. Constantinidis I, Grant S, Simpson NE, Oca-Cossio JA, Sweeney CA, Mao H, Blackband SJ, Sambanis A. Use of magnetic nanoparticles to monitor alginate-encapsulated betaTC-tet cells. Magn Reson Med. 2009; 61(2):282–290. [PubMed: 19165877]
25. Feng Y, Jeong EK, Mohs AM, Emerson L, Lu ZR. Characterization of tumor angiogenesis with dynamic contrast-enhanced MRI and biodegradable macromolecular contrast agents in mice. Magn Reson Med. 2008; 60(6):1347–1352. [PubMed: 19025902]
26. Tweedle MF, Wedeking P, Kumar K. Biodistribution of radiolabled, formulated gadopentetate, gadoteriol, gadoterate and gadodiamide in mice and rats. Invest Radiol. 1995; 30(6):372–380. [PubMed: 7490190]
27. Tweedle MF. Physicochemical properties of gadoteridol and other magnetic resonance contrast agents. Invest Radiol. 1992; 27 Suppl. 1:2–6. [PubMed: 1733876]
28. Abraham JL, Thakral C. Tissue distribution and kinetics of gadolinium and nephrogenic systemic fibrosis. Eur J Radiol. 2008; 66(2):200–207. [PubMed: 18374532]
29. Zak O, Aisen P. Spectroscopic and thermodynamic studies on the binding of gadolinium(III) to human serum transferrin. Biochemistry. 1988; 27(3):1075–1080. [PubMed: 2835077]
30. Bass LA, Wang M, Welch MJ, Anderson CJ. In vivo transchelation of copper-64 from TETA-octreotide to superoxide dismutase in rat liver. Bioconjugate Chem. 2000; 11:527–532.
31. Franano FN, Edwards WB, Welch MJ, Brechbiel MW, Gansow OA, Duncan JR. Biodistribution and metabolism of targeted and nontargeted protein-chelate-gadolinium complexes: evidence for

gadolinium dissociation in vitro and in vivo. Magn Reson Imaging. 1995; 13(2):201–214. [PubMed: 7739361]

32. Hocine N, Berry JP, Jaafoura H, Escaig F, Masse R, Galle P. Subcellular localization of gadolinium injected as soluble salt in rats: a microanalytical study. Cell Mol Biol. 1995; 41(2): 271–278. [PubMed: 7787737]
33. Darrah TH, Prutsman-Pfeiffer JJ, Poreda RJ, Campbell ME, Hauschkac PV, Hannigand RE. Incorporation of excess gadolinium into human bone from medical contrast agents. Metallomics. 2009; 1:479–488. [PubMed: 21305156]
34. Frenzel T, Lengsfeld P, Schirmer H, Huetter J, Weinmann H-J. Stability of gadolinium-based magnetic resonance imaging contrast agents in human serum at 37°C. Invest Radiol. 2008; 43(12): 817–828. [PubMed: 19002053]
35. Anderson CJ. Metabolism of radiometal-labeled proteins and peptides: What are the real radiopharmaceuticals *in vivo*? Cancer Biother Radiopharm. 2001; 16(6):451–455. [PubMed: 11789022]

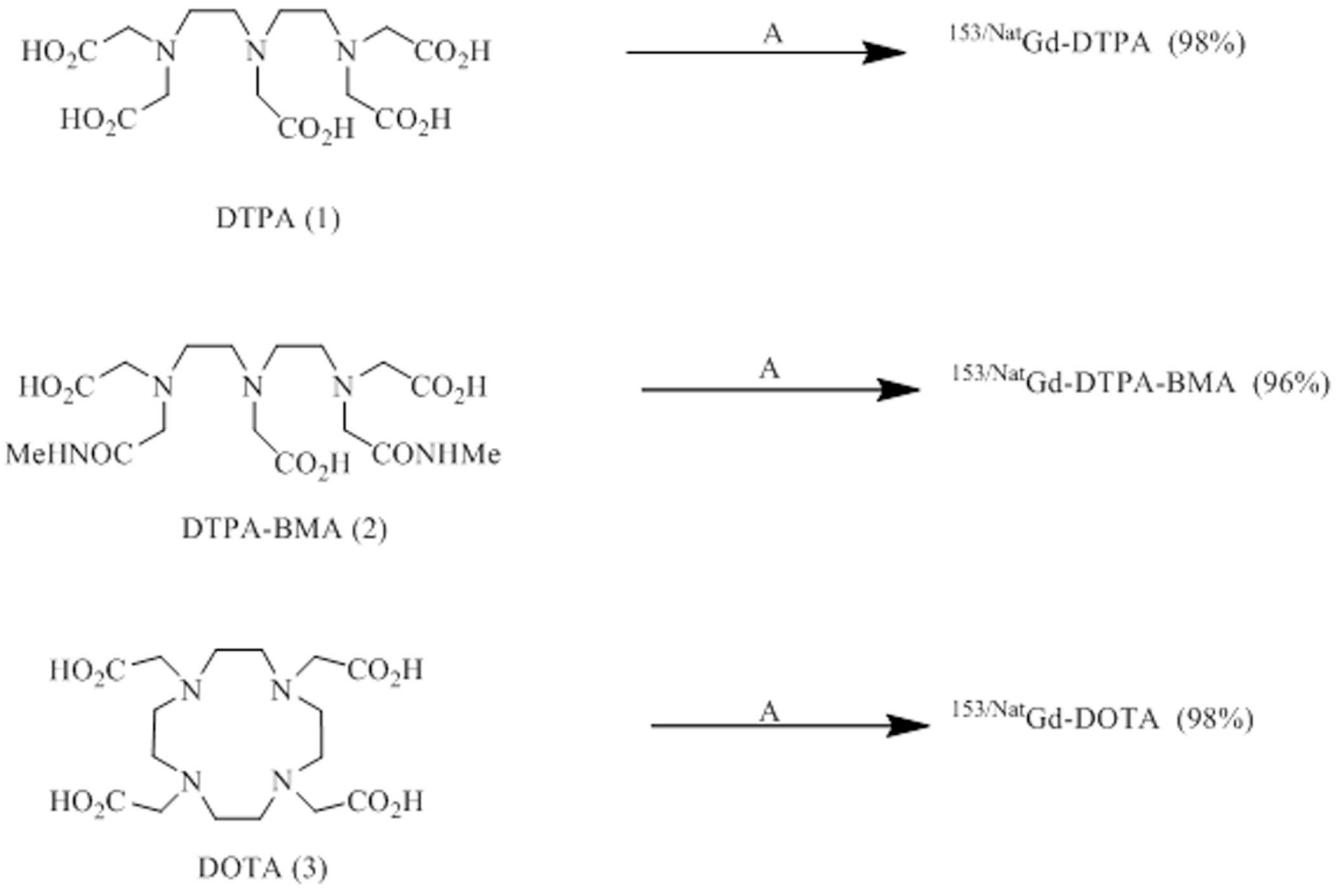

Figure 1.
Synthetic scheme detailing the preparation of $^{153/Nat}$Gd-DOTA, $^{153/Nat}$Gd-DTPA and $^{153/Nat}$Gd-DTPA-BMA.

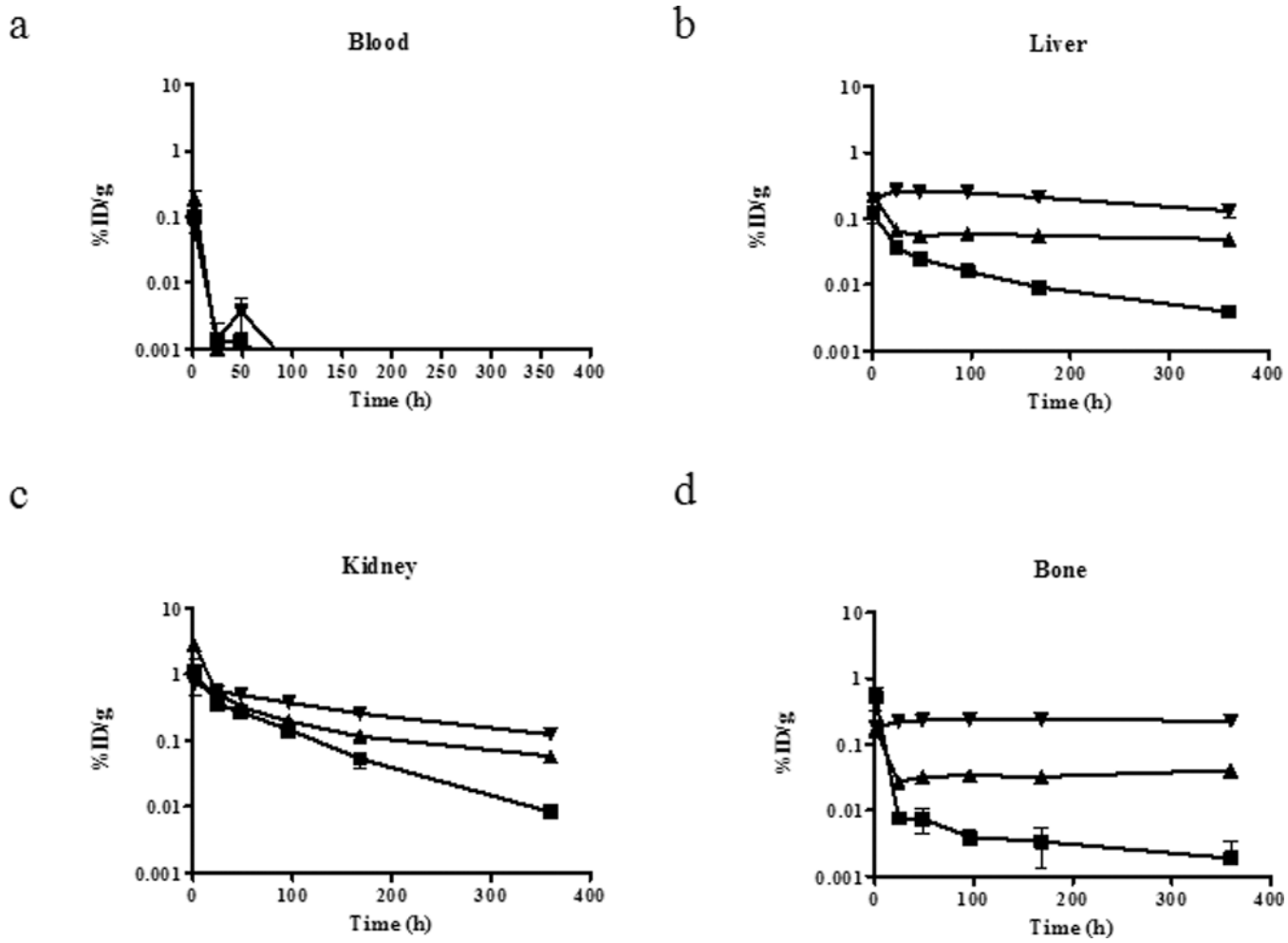

Figure 2.

Biodistribution results of $^{153/Nat}$Gd-DOTA (■), $^{153/Nat}$Gd-DTPA-BMA (▼) and $^{153/Nat}$Gd-DTPA (▲) in WT mice over time. Selected tissues are presented, and note the scale differences in the y-axes, which are displayed on a log scale. The mean ± SD is displayed at each time point, but error bars representing the SD may not be observed if it is small. Even after 15 days, more activity is observed in the tissues of mice that received $^{153/Nat}$Gd-DTPA-BMA and suggests that this complex is not as stable *in vivo* as $^{153/Nat}$Gd-DOTA and $^{153/Nat}$Gd-DTPA.

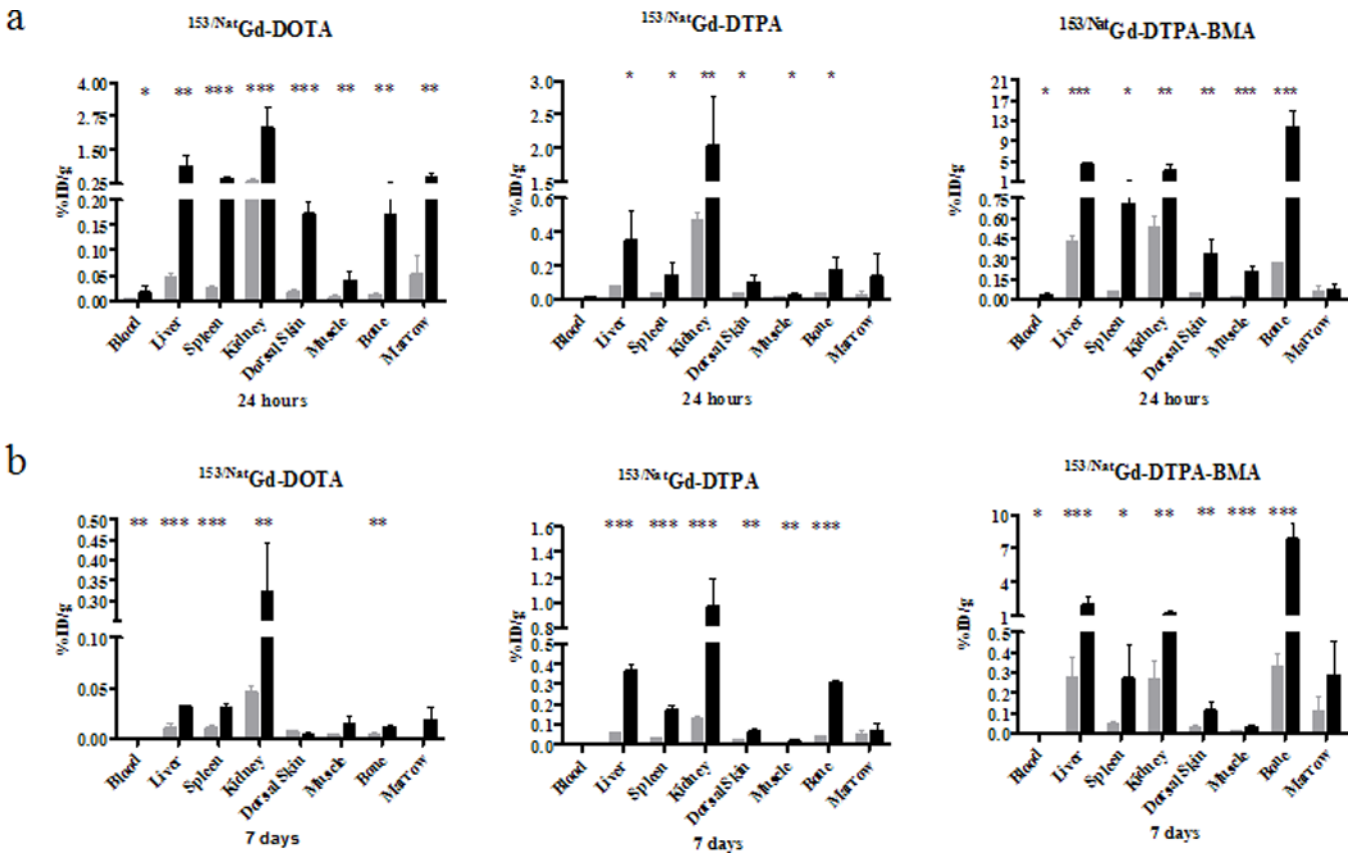

Figure 3.

Biodistribution results of $^{153/Nat}$Gd-DOTA, $^{153/Nat}$Gd-DTPA and $^{153/Nat}$Gd-DTPA-BMA in selected tissues of control (

) and RI mice (■) at 24 hours (a) and 7 days (b). Please note the scale differences in the y-axes. Asterisks denote statistical significance (* = $p < 0.05$, ** = $p < 0.01$, *** = $p < 0.001$). RI mice have significantly more ^{153}Gd associated with their tissues even after 7 days suggesting that renal impairment allows for a longer circulation time of the contrast agents and provides an opportunity for Gd-chelate dissociation thereby increasing the probability that Gd ions will be free to interfere with normal biochemical pathways.

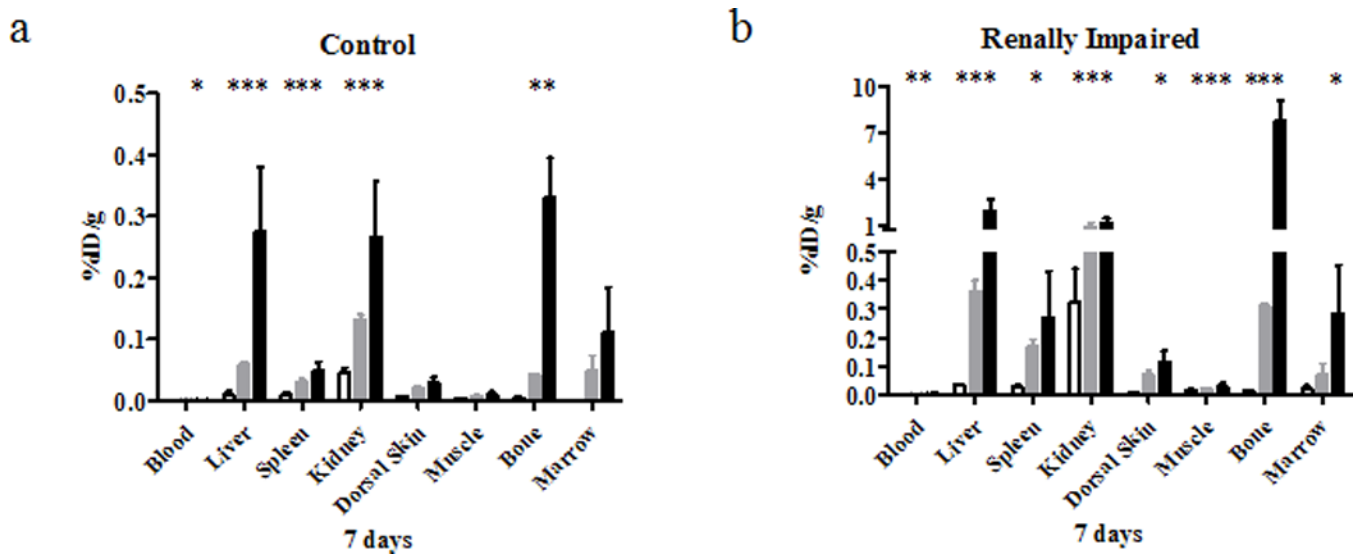

Figure 4.

Biodistribution results of $^{153/Nat}$Gd-DOTA (□), $^{153/Nat}$Gd-DTPA (▒) and $^{153/Nat}$Gd-DTPA-BMA (■) in selected tissues of control (a) and RI (b) mice at 7 days. Please note the scale differences in the y-axes. Asterisks denote statistical significance (* = $p < 0.05$, ** = $p < 0.01$, *** = $p < 0.001$). Based upon this comparison of the radiotracers, it is observed that $^{153/Nat}$Gd-DTPA-BMA demonstrated the greatest instability generating more tissue associated activity. The magnitude of the tissue associated activity increases significantly in the renally impaired animals and demonstrates how renal impairment may magnify the effects of Gd-chelate instability.